ELSEVIER

Polymer 44 (2003) 2373–2377

polymer

www.elsevier.com/locate/polymer

Crystallization and orientation studies in polypropylene/single wall carbon nanotube composite

Arup R. Bhattacharyya[a,1], T.V. Sreekumar[a], Tao Liu[a], Satish Kumar[a,*], Lars M. Ericson[b], Robert H. Hauge[b], Richard E. Smalley[b]

[a]*School of Textile and Fiber Engineering, Georgia Institute of Technology, Atlanta, GA 30332, USA*
[b]*Center for Nanoscale Science and Technology, Rice University, Houston, TX 77005, USA*

Received 22 May 2002; received in revised form 4 November 2002; accepted 15 January 2003

Abstract

Crystallization behavior of melt-blended polypropylene (PP)/single wall carbon nanotube (SWNT) composites has been studied using optical microscopy and differential scanning calorimetry. Polypropylene containing 0.8 wt% SWNT exhibits faster crystallization rate as compared to pure polypropylene. PP/SWNT fibers have been spun using typical polypropylene melt spinning conditions. The PP crystallite orientation and the SWNT alignment in the fibers have been studied using X-ray diffraction and polarized Raman spectroscopy, respectively.

Keywords: Polypropylene; Single wall carbon nanotubes; Crystallization

1. Introduction

Polypropylene mechanical properties are generally modified by melt mixing with particulate (talc, mica, clay) [1–4] and fibrous (glass, jute, aramid, and carbon fibers) fillers [5–9] as well as by melt blending with other polymers [10–13]. Reinforcement at nanoscale to improve mechanical and other properties including changes in polymer crystallization behavior is being attempted [14–20]. Addition of nanostructured polyhedral silsesquioxane (POSS) [16], vapor grown carbon nanofibers [17], as well as montmorillonite clay [19] increased the crystallization rate of polypropylene. Single wall carbon nanotubes (SWNTs) due to their high tensile strength and modulus [21–23] are excellent candidates for nano-reinforcement of a variety of polymer matrices. Examples of mechanical property improvements using nano-reinforcement include polypropylene/carbon nanofiber [18], pitch/SWNT [24], PMMA/SWNT [25] and PBO/SWNT fibers [26]. Here we report the crystallization behavior of PP in the presence of SWNTs, as well as the alignment of SWNT in the polypropylene matrix.

2. Experimental

Amoco polypropylene powder (#107200) with a melt flow index (MFI) of 17 and purified SWNTs obtained from Rice University's HiPco™ process were used in this study [27,28]. Polypropylene with 1 wt% SWNT was mixed in a Haake rheomix 600 mixer at 240 °C at 50 rpm for 30 min. A control polypropylene sample without nanotube was also processed in the Haake mixer under the same conditions. Both the PP/SWNT composite as well as pure PP melts were filtered by passing through a 300, 250, 120 and 80 mesh stainless steel filter assembly at 240 °C. After filtration, the SWNT content in polypropylene was reduced to 0.8 wt% as determined from thermogravimetric analysis (TGA), which was carried out on a TA instruments' TGA 2950 at 10 °C/min under nitrogen. The SWNT weight reduction represents filtration of larger SWNT agglomerates. PP and PP/SWNT crystallization was observed using Leitz polarizing microscope equipped with a hot stage. Samples were allowed to cool down to room temperature after holding them at 240 °C for 5 min. For DSC study using TA Instruments' DSC

* Corresponding author. Tel.: +1-404-894-2490; fax: +1-404-894-8780.
E-mail address: satish.kumar@textiles.gatech.edu (S. Kumar).
[1] Present address: Institute of Polymer Research Dresden, Hohe Strasse 6, D-01069 Dresden, Germany

0032-3861/03/$ - see front matter © 2003 Elsevier Science Ltd. All rights reserved.
doi:10.1016/S0032-3861(03)00073-9

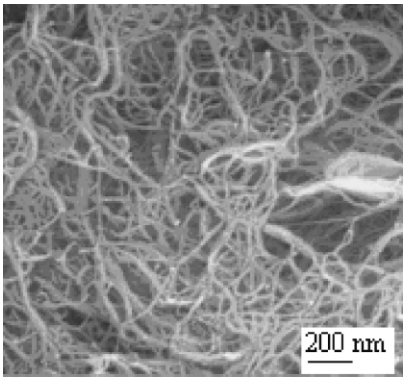

Fig. 1. Scanning electron micrograph of SWNT powder.

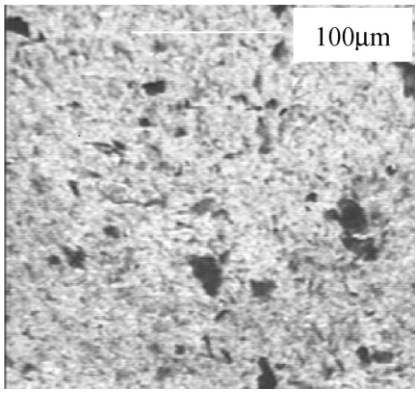

Fig. 2. Optical micrograph (without cross-polars) of polypropylene/SWNT composite containing 0.8 wt% SWNTs.

Q100, samples were heated at 10 °C/min to 240 °C and cooled at the same rate. The first cooing and second heating DSC traces were used for analysis. The crystallization kinetics study using DSC, samples were quenched from 240 °C at 80 °C/min to the desired crystallization temperature, at which the heat flow for isothermal crystallization was monitored.

The crystallization kinetics was studied using the Avrami equation [29]:

$$\ln\{-\ln[1-X(t,T)]\} = \ln k(T) + n \ln t$$

where $X(t,T)$ is the crystalline fraction of the material at time, t, with respect to the total crystallinity at infinite time at isothermal crystallization temperature (T); n and k are the Avrami crystallization parameters. Half crystallization time, $t_{1/2}$, was obtained from the equation $t_{1/2} = [\ln 2/k]^{1/n}$.

PP as well as PP/SWNT fibers were melt-spun at 240 °C using a spinning unit manufactured by Bradford University Ltd, UK. The fibers were subsequently drawn to the maximum achievable draw ratio of 4.5 at 130 °C. The polarized Raman spectra were collected in the back scattering geometry using a Holoprobe Research 785 Raman Microscope made by Kaiser Optical System Inc., using 785 nm wavelength laser. Measurements were made when fiber was at 0°, 5°, 15°, 30°, 45°, 60°, 75°, and 90° to the polarization direction of the excitation laser source. At each angle, both the VV and VH spectra were collected. In the VV configuration, the polarizer and the analyzer are parallel to each other; and in the VH configuration, the polarizer and the analyzer are perpendicular to each other. Fiber tensile properties were measured using Instron tensile tester at 2.54 cm gauge length at a strain rate of 100% per minute. X-Ray diffraction studies were carried out using the synchrotron source at Brookhaven National Laboratory (X-ray wavelength, 0.1542 nm).

3. Results and discussion

The individual SWNT diameter determined from Raman spectroscopy was in the 0.77–1.16 nm range. The individual nanotubes rope into bundles or fibrils, which have an average rope/fibril diameter of about 40 nm as seen by SEM (Fig. 1). TGA (not shown) of this purified SWNT powder in air showed 7 wt% residue above 800 °C and is a result of the catalytic impurity remaining after purification. Catalytic impurity in the as produced HiPco™ SWNTs is typically above 20 wt%. Using the continuous purification process, HiPco™ SWNTs with purity greater than 99% have been obtained [26].

The optical micrograph of the PP/SWNT composite in the melt state (Fig. 2) shows significant nanotube aggregates.

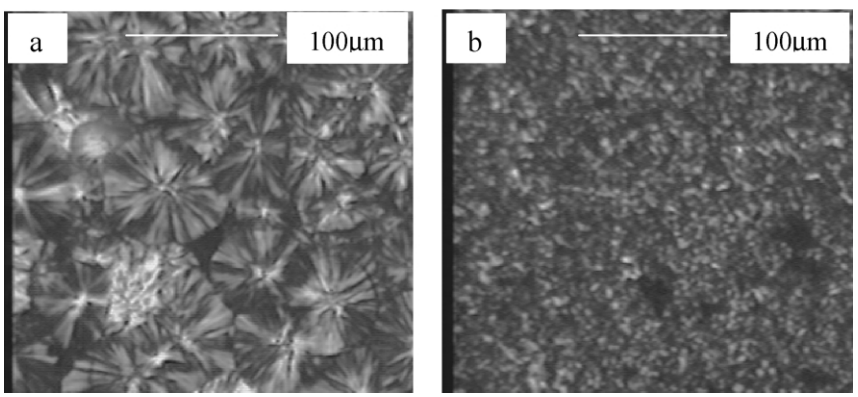

Fig. 3. Optical micrographs (with cross-polars) of (a) polypropylene and (b) PP/SWNT composite containing 0.8 wt% SWNTs.

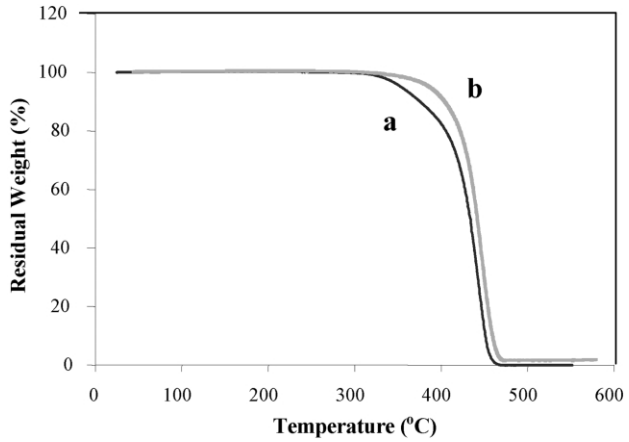

Fig. 4. TGA plots of (a) PP and (b) PP/SWNT composite in nitrogen at a heating rate of 10 °C/min.

Crystallization behavior as observed from optical microscopy is shown in Fig. 3. The spherulite size in polypropylene is much larger than in PP/SWNT, suggesting that nanotube ropes or nanotube aggregates act as nucleating sites for polypropylene crystallization. However, the issue of the development of transcrystallinity has not been addressed in this study. The residual weight (0.8%) in the TGA study of PP/SWNT composite in Fig. 4 above 500 °C represents the weight of the SWNT. DSC scans in Fig. 5 show that when cooled at 10 °C/min, polypropylene crystallized at 114.5 °C, while crystallization in PP/SWNT occurred at 125.8 °C. In addition, both the melting and crystallization peaks in PP/SWNT composite are narrower than in pure polypropylene. For example, the full width at half maximum for PP and PP/SWNT crystallization peaks are 5.7 and 4.4 °C, respectively. Narrower crystallization and melting peak would suggest a narrower crystallite size distribution in the PP/SWNT composite as compared to pure polypropylene. A narrower melting peak was also observed in the PET/nanocarbon fiber composite as compared to pure PET [30]. Higher thermal conductivity of the carbon

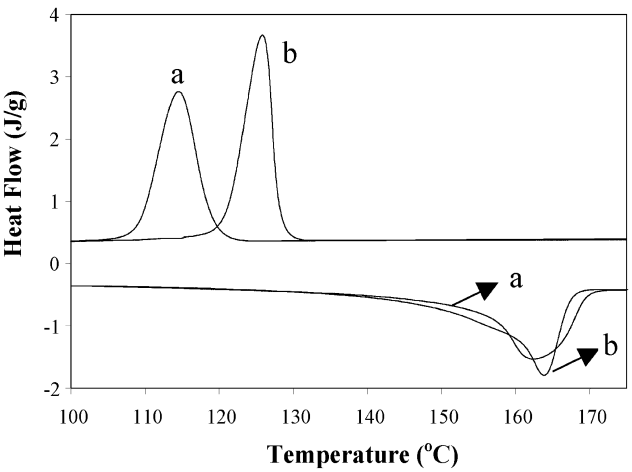

Fig. 5. DSC cooling (first cycle) and heating (second cycle) curves for (a) PP and (b) PP/SWNT composite containing 0.8 wt% SWNTs.

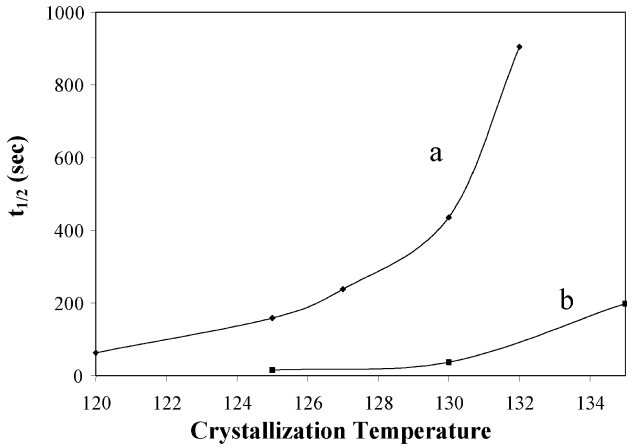

Fig. 6. Crystallization half time ($t_{1/2}$) of (a) polypropylene and (b) PP/SWNT (99.2/0.8) as a function of crystallization temperature.

nanotubes as compared to that of the polymer, at least in part may be responsible for the sharper crystallization and melting peaks, as heat will be more evenly distributed in the samples containing the carbon nanotubes.

Polypropylene in the β-crystal form melts at lower temperature than the α-crystals [31]. A peak at about 165 °C in Fig. 5(b) is attributed to the melting of α-crystals in PP/SWNT and the appearance of broad peak in the 145–160 °C temperature range can be due to the melting of β-crystals, or smaller or imperfect α-crystals. However, as discussed later, X-ray diffraction of the PP/SWNT fiber does not show the presence of β-crystals. Enthalpy of melting for PP and PP/SWNT composites from the second heating curves was 93 and 100 J/g, respectively.

The half crystallization time as a function of isothermal crystallization temperature is given in Fig. 6 and the isothermal crystallization parameters (n and k) determined by the Avrami equation are given in Table 1. A value close to 3 for the Avrami exponent implies a three-dimensional heterogeneous crystal growth and is practically unchanged with the addition of SWNTs. The addition of 0.8 wt% SWNT increases the crystallization rate by as much as an order of magnitude or higher and is attributed to enhanced nucleation, resulting from the presence of SWNTs.

SWNTs show resonance-enhanced Raman scattering effect when a visible or near infrared laser is used as the excitation source [32–34] and polypropylene as well as most other polymers do not show such a resonance effect. Therefore, the Raman spectroscopy is an ideal characterization technique for the orientation study of SWNT [25,35].

Table 1
Isothermal crystallization parameters for PP and PP/SWNT composite

Sample	125 °C		130 °C	
	n	K (s^{-1})	n	K (s^{-1})
PP	3.4	1.8×10^{-8}	2.8	2×10^{-8}
PP/SWNT	3.5	4.2×10^{-5}	3.4	2.7×10^{-6}

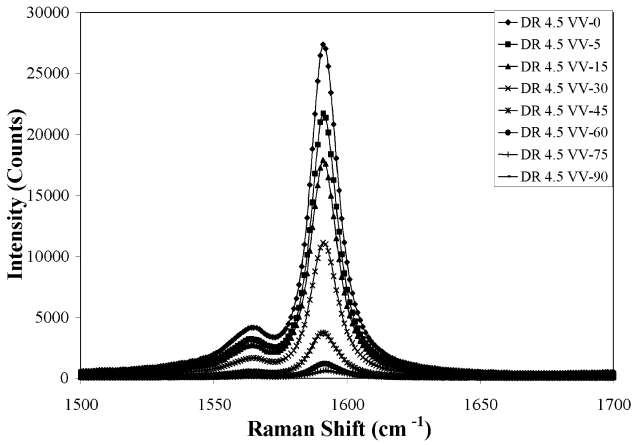

Fig. 7. Tangential mode Raman spectra of PP/SWNT composite fiber (draw ratio = 4.5) under VV configuration. From top to bottom, the angle between fiber axis and polarization direction of polarizer is 0°, 5°, 15°, 30°, 45°, 60°, 75°, and 90°.

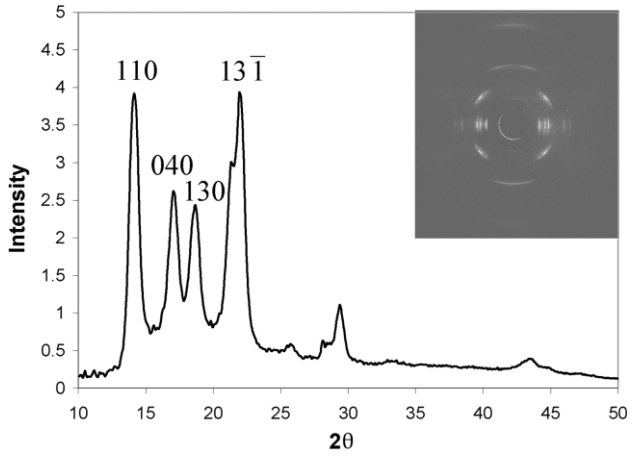

Fig. 8. Integrated wide angle X-ray diffraction intensity of PP/SWNT composite fiber (draw ratio = 4.5). Inset: 2D X-ray image for the same sample.

In Refs. [25,35], the orientation of SWNT was treated as if they were distributed around the fiber axis in a 2D plane. While 3D distribution depicts fiber cylindrical symmetry more accurately [36,37], for simplicity, we have also used 2D distribution approximation to study the orientation of SWNTs in PP/SWNT composite fibers. Fig. 7 shows the tangential mode Raman spectra (1500–1700 cm^{-1}) of the SWNT/PP composite fiber with a draw ratio of 4.5 at VV configuration, where the Raman scattering intensity monotonically decreases with increasing the angle between the fiber axis and the polarization direction of the polarizer. Using the height of 1592 cm^{-1} peak and based on the Gaussian distribution, Herman's orientation factors[1] of SWNT in PP/SWNT composite fibers were 0.81 and 0.95 for the as spun and the drawn fiber (draw ratio 4.5), respectively. Herman's orientation factor was also calculated using Lorentzian distribution, and the corresponding orientation factor values for the as spun and drawn fibers were 0.72 and 0.92, respectively. The orientation factor calculated from Lorentzian intensity distribution is lower than that calculated from Gaussian function and the difference between them diminishes with increasing SWNT orientation. This is due to the fact that the Lorentzian function is more weighted on the tail than the Gaussian function. A mixed Lorentzian and Gaussian function may be a better distribution function for the orientation of SWNT in SWNT/PP composite fiber. A detailed SWNT orientation study in fibers will be published elsewhere [38].

Fig. 8 shows 1D integrated X-ray diffraction intensity profile of the drawn SWNT/PP fiber of 4.5 draw ratio, which is extracted from its 2D wide angle X-ray image shown in the inset of Fig. 8. The integrated X-ray diffraction intensity of SWNT/PP shows the typical α-form PP crystals and exhibited complete absence of the β-crystal form, which shows [39] two strong peaks at 2θ of 16.2° and 21.2°. While certain nucleating agents can promote β-crystal formation in polypropylene [39], this study shows only the α-crystal formation in PP/SWNT composite. In addition, the diffraction of SWNT bundles, which posses a 2D hexagonal lattice structure [40,41], was also not observed.

From the X-ray diffraction of drawn SWNT/PP fiber, the Herman's orientation factors for (040) and (110) PP planes were calculated to be −0.40 and −0.45, respectively. The Herman's orientation factor for the (001) plane determined using the Wilchinsky equation [42] is 0.86. Compared to the Herman's orientation factor of SWNT (0.92 for the Lorentzian distribution and 0.95 for Gaussian distribution) in SWNT/PP fiber of same draw ratio, PP shows somewhat lower orientation. This is expected to be a result of higher PP chain flexibility as compared to SWNT.

For effective reinforcement, good nanotube dispersion is necessary. Data in Table 2 show that the fiber mechanical properties are mostly unaffected with the presence of SWNTs. Micrometer size single wall nanotube (SWNT) aggregates (Fig. 2) in PP/SWNT composite did not negatively affect the mechanical properties. This would suggest that such large nanotube aggregates either did not act as stress concentrators, or if they did act as stress concentrator, their effect was nullified by those nanotubes or nanotube ropes that may be well dispersed, providing effective reinforcement. When carbon nanotubes are well dispersed in polymer matrix, improvements in mechanical

Table 2
Mechanical properties of PP and PP/SWNT composite fibers of 4.5 draw ratio

Fiber	Diameter	Tensile strength (GPa)	Modulus (GPa)	Elongation to break (%)
PP	30 ± 2	0.43 ± 0.1	4.2 ± 1.2	36 ± 15
PP/SWNT	28 ± 2	0.42 ± 0.1	4.0 ± 1.0	27 ± 8

[1] Herman's orientation factor (f) is given by $f = (3\langle\cos^2\theta\rangle - 1)/2$, where θ is the angle between the orienting entity and the fiber axis.

properties are observed. Examples include 50% increase in PP fiber modulus with the addition of 5 wt% carbon nanofibers [18], and 60% increase in PBO fiber tensile strength with the addition of 10 wt% SWNT [26]. It is noted that improved tensile strength PBO/SWNT fibers were obtained when SWNT with >99% purity were used. Fibers processed with high catalytic impurity resulted in lower tensile strength [43]. With good SWNT dispersion and purity, similar tensile strength improvements in PP and other polymers can be expected. Current efforts are aimed at improving nanotube dispersion in polypropylene and other polymer matrix systems.

4. Conclusions

Purified HiPco SWNTs exhibit poor dispersion when melt blended with PP. SWNT, even with poor dispersion act as nucleating agent for PP crystallization, and WAXD studies show no evidence of polypropylene β-crystal formation. WAXD and Raman spectroscopy studies show that in the drawn PP/SWNT composite fiber, SWNTs have higher orientation than PP.

Acknowledgements

Financial support for this work from the Office of Naval Research and the development of HiPco™ process at Rice University from the Office of Naval Research, NASA, the Texas Advanced Technology Program, and the Robert A. Welch Foundation is gratefully acknowledged. We are grateful to Drs B.S. Hsiao and S. Ran for the X-ray diffraction.

References

[1] Velasco JI, De Saja JA, Martinez AB. J Appl Polym Sci 1996;61:125.
[2] Liu X, Wu Q. Polymer 2001;42:10013.
[3] Qiu W, Mai K, Zeng H. J Appl Polym Sci 2000;77:2974.
[4] Chiang WY, Yang WD, Pukanszky B. Polym Engng Sci 1994;34:485.
[5] Kuhnert I, Fischer HD, Muras J. Kunstoff 1997;42:29.
[6] Wu C-M, Chen M, Karger-Kocsis J. Polymer Bull 1998;41:239.
[7] Assouline E, Pohl S, Fulchiron R, Gerard J-F, Lustiger A, Wagner HD, Marom G. Polymer 2000;41:7843.
[8] Hobbs SY. Nat Phys Sci 1971;234:12.
[9] Campbell D, Qayyum MM. J Polym Sci, Polym Phys Ed 1980;18:83.
[10] Duvall J, Sellitti C, Myers C, Hiltner A, Baer E. J Appl Polym Sci 1994;52:195.
[11] Ikkala OT, Holsti-Miettinen RM, Seppala I. J Appl Polym Sci 1993; 49:1165.
[12] Gupta AK, Purwar SN. J Appl Polym Sci 1984;29:1595.
[13] Zhang X, Xie F, Pen Z, Zhang Y, Zhang Y, Zhou W. Eur Polym J 2002;38:1.
[14] Thostenson ET, Ren Z, Chou T-W. Composites Sci Technol 2001;61: 1899.
[15] Fornes TD, Yoon PJ, Keskkula H, Paul DR. Polymer 2001;42:9929.
[16] Fu BX, Yang L, Somani RH, Zong SX, Hsiao BS, Phillips S, Blanski R, Ruth P. J Polym Sci Part B: Polym Phys 2001;39:2727.
[17] Lozano K, Barrera EV. J Appl Polym Sci 2001;79:125.
[18] Kumar S, Doshi H, Srinivasrao M, Park JO, Schiraldi DA. Polymer 2002;43:1701.
[19] Ma J, Zhang S, Qi Z, Li G, Hu Y. J Appl Polym Sci 2002;83:1978.
[20] Zhang M, Liu Y, Zhang X, Gao J, Huang F, Song Z, Wei G, Qiao J. Polymer 2002;43:5133.
[21] Yakobson BI, Smalley RE. Am Sci 1997;85:324.
[22] Yu MF, Files BS, Arepalli S, Ruoff RS. Phys Rev Lett 2000;84(24): 5552.
[23] Baughman RH, Zakhidov AA, de Heer WA. Science 2002;297:787.
[24] Andrews R, Jacques D, Rao AM, Rantell T, Derbyshire F, Chen Y, Chen J, Haddon RC. Appl Phys Lett 1999;75:1329.
[25] Haggenmueller R, Gommans HH, Rinzler AG, Fischer JE, Winey KI. Chem Phys Lett 2000;330:219.
[26] Kumar S, Dang TD, Arnold FE, Bhattacharyya AR, Min BG, Zhang X, Vaia RA, Park C, Adams WW, Hauge RH, Smalley RE, Ramesh S, Willis PA. Macromolecules 2002;35:9039.
[27] Nikolaev P, Bronikowski MJ, Bradley RK, Rohmund F, Colbert DT, Smith KA, Smalley RE. Chem Phys Lett 1999;313:91.
[28] Chiang IW, Brinson BE, Huang AY, Willis PA, Bronikowski MJ, Margrave JL, Smalley RE, Hauge RH. J Phys Chem B 2001;105: 8297.
[29] Avrami M. J Chem Phys 1939;7:1103.
[30] Ma H, Zeng J, Realff ML, Kumar S, Schiraldi DA. Composites Sci Technol, in press.
[31] Mandelkern L, Alamo RG. Physical properties of polymers handbook. In: Mark JE, editor. American Institute of Physics; 1996. p. 123.
[32] Dresselhaus MS, Eklund PC. Adv Phys 2000;49:705.
[33] Pimenta MA, Marucci A, Empedocles SA, Bawendi MG, Hanlon EB, Rao AM, Eklund PC, Smalley RE, Dresselhaus G, Dresselhaus MS. Phys Rev B 1998;58:R16016.
[34] Brown SDM, Jorio A, Corio P, Dresselhaus MS, Dresselhaus G, Satio R, Kneipp K. Phys Rev B 2001;63:155411–4.
[35] Hwang J, Gommans HH, Ugawa A, Tashiro H, Haggenmueller R, Winey KI, Fischer JE, Tanner DB, Rinzler AG. Phys Rev B 2000;62: R13310.
[36] Anglaret E, Righi A, Sauvajol JL, Bernier P, Vigolo B, Poulin P. Phys Rev B 2002;65:165421–6.
[37] Anglaret E, Righi A, Sauvajol JL, Bernier P, Vigolo B, Poulin P. Physica B 2002;323:38.
[38] Liu T, et al., in press.
[39] Ellis G, Gomez MA, Marco C. The internet journal of vibrational spectroscopy, vol. 5, 4th ed, Section 5.
[40] Thess A, Lee R, Nikolaev P, Dai H, Petit P, Robert J, Xu C, Lee YH, Kim SG, Rinzler AG, Golbert DT, Scuseria GE, Tomanek D, Fischer JE, Smalley RE. Science 1996;273:483.
[41] Wei B, Vajtai R, Choi YY, Ajayan PM, Zhu H, Xu C, Wu D. Nano Lett 2002;2:1105.
[42] Samuels RJ. Structured polymer properties. New York: Wiley; 1974. p. 28–37.
[43] Kumar S, et al. Unpublished results.